Eur. Phys. J. Appl. Phys. **97**, 21 (2022)

https://doi.org/10.1051/epjap/2022210237

THE EUROPEAN PHYSICAL JOURNAL APPLIED PHYSICS

Regular Article

The effects of alkaline-earth-metal-element doping on the thermoelectric properties of β-Zn_4Sb_3★

Mian Liu[1,2,*], Changsong Liu[3], and Xiaoying Qin[3,*]

[1] Center for Magnetic Materials and Devices, College of Physics and Electronic Engineering, Qujing Normal University, Qujing 655011, P.R. China
[2] Key Laboratory for Advanced Functional and Low Dimensional Materials of Yunnan Higher Education Institute, Qujing Normal University, Qujing 655011, P.R. China
[3] Key Laboratory of Materials Physics, Institute of Solid State Physics, Chinese Academy of Sciences, P.O. Box 1129, Hefei 230031, P.R. China

Received: 19 October 2021 / Received in final form: 23 December 2021 / Accepted: 3 February 2022

Abstract. The effects of alkaline-earth metal elements Ca, Sr, and Ba on the electronic structure and thermoelectric properties of β-Zn_4Sb_3 were investigated by performing self-consistent ab initio electronic structure calculations within density functional theory and solving the Boltzmann transport equations within the relaxation time approximation. The results demonstrate that these alkaline-earth metal elements with *s* orbitals could introduce giant sharp resonant peaks in the electronic density of states (DOS) near the host valence band maximum in energy. And these deliberately engineered DOS peaks result in a sharp increase of the room-temperature Seebeck coefficient of β-Zn_4Sb_3 by a factor of nearly 8/9/19, respectively. Additionally, with the simultaneous increase of conductivity and decline of carrier thermal conductivity upon Ca/Sr/Ba doping, potentially, at least, 10/4/2-fold increase in optimizing power factor, and 14/12/8-fold increase in thermoelectric figure of merit of β-Zn_4Sb_3 at room temperature are achieved. And their corresponding optimal Fermi levels are all located near the host valence band maximum.

1 Introduction

Because of the capability of directly converting waste heat into electricity without causing environmental pollution, there has been a renewed interest toward thermoelectric materials driven by energy crisis and the environment issues currently [1–8]. The energy conversion efficiency of thermoelectric materials is determined by the dimensionless figure of merit $ZT = S^2\sigma T/\lambda$, where S is the Seebeck coefficient, σ is the electrical conductivity, λ ($=\lambda_C+\lambda_L$) is thermal conductivity with both the carrier (λ_C) and lattice (λ_L) contributions, and T is the absolute temperature. "phonon glass-electron crystal" thermoelectric property [9] was recognized as the characteristic of an ideal thermoelectric material.

Recently, β-Zn_4Sb_3, with a $ZT = 1.3$ at 670 K and an extraordinarily low thermal conductivity (~0.7 $Wm^{-1}K^{-1}$ at 650 K) [10], has been claimed to be a potential highly efficient thermoelectric material for commercial application in the moderate temperature range. The crystal structure of β-Zn_4Sb_3 contains three distinct atomic positions (36 Zn, 18 Sb(1), and 12 Sb(2) in space group R3c with disordered vacancies and interstitial Zn atoms [11–13].

Recent research indicated that thermoelectric performance of β-Zn_4Sb_3 could be improved through appropriate doping. For instance, dopants such as Pb, Bi, Mg, Cu, Sn, In, Cd, Al, Ga, Nb, Hg and Ag have been investigated so far [14–29]. And, the most results showed that the enhanced thermoelectric performance are mainly due to a reduction in thermal conductivity. However, the thermal conductivity of the parent compound β-Zn_4Sb_3 is very low ($< 1\,W\,m^{-1}\,K^{-1}$) [10,24,30] which is close to the theoretical minimum for the thermal conductivity in solids [11]. Therefore, in the present work, we focused our attention on improving its power factor ($=S^2\sigma$) by doping alkaline-earth metal elements (here Ca, Sr and Ba) through a systematic study on the structural properties and thermoelectric properties of substituted β-Zn_4Sb_3 system with density functional theory and Boltzmann transport theory.

2 Computational methods

According to the recent study on β-Zn_4Sb_3 [10,11,30–35], its true crystal structure was presented in Figure 1 of Supplementary Material. The actual composition of β-Zn_4Sb_3 is $Zn_{13-\delta}Sb_{10}$ ($\delta = 0.2$–0.5), a slight Zn deficiency in respect to the ideal crystallographic composition $Zn_{13}Sb_{10}$ [36]. A considerable occupational deficiency (0.89–0.90) and three weakly occupied (by around 0.06) interstitial Zn atoms [11,12] in this material manifest a

★ Supplementary material is available in electronic form at https://www.epjap.org/0.1051/epjap/2022210237

* e-mail: liumianytu@163.com; xyqin@issp.ac.cn

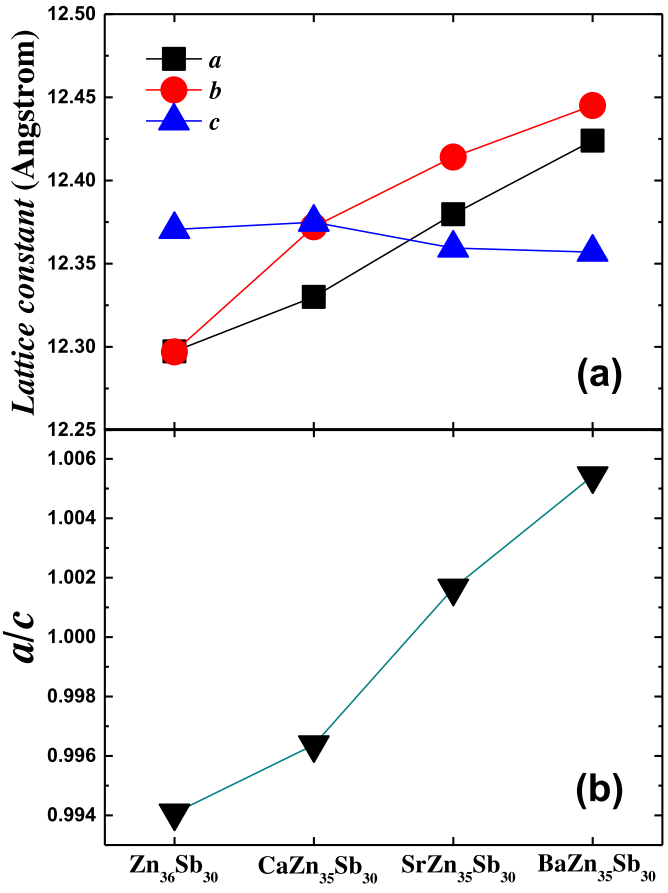

Fig. 1. (a) Variation in lattice constants and (b) their ratio a/c of $Zn_{36}Sb_{30}$ without doping and doping Ca/Sr/Ba.

disordering in the framework Zn position, which brings an insurmountable difficulty to theoretical simulation. Hence, for simplicity, we based on Cargnoni's model [12] and utilized a framework of $Zn_{36}Sb_{30}$, a hypothetical disorder-free β-Zn_4Sb_3, to simplify the practical structure of β-Zn_4Sb_3. Then the Zn-substituted compounds can be expressed as $MZn_{35}Sb_{30}$ (M = Ca/Sr/Ba).

Our calculations are performed with Vienna ab initio simulation package (VASP) [37–39], based on the density-functional theory, using the PBE generalized gradient approximation to the exchange correlation energy, and projector augmented wave potential for the valence electron-ion interaction. The energy cutoff for the plane wave expansion was 350 eV. The ionic coordinates and the unit cell's size and shape were optimized simultaneously until all the forces converge to below 0.001 eV/Å.

Electrical transport properties, σ, S and λ_C were calculated based on the ab initio calculation results, within the framework of the Boltzmann transport theory as the following expressions [40,41]:

$$\sigma = e^2 L^{(0)} \tag{1a}$$

$$S = -L^{(1)}/\left(eTL^{(0)}\right) \tag{1b}$$

$$\lambda_C = 1/TL^{(2)} - S^2\sigma T \tag{1c}$$

$$L^{(a)} = \int_{-\infty}^{+\infty} dE\left(-\frac{\partial f_0}{\partial E}\right) g(E)v(E)^2\tau(E)(E-E_f)^a \tag{1d}$$

here f_0, e, $g(E)$, $\upsilon(E)$, E_f, k, and τ is Fermi distribution function, the electron charge, density of states, electron velocity, Fermi energy, electron wave vector, and total relaxation time, respectively. Polar scattering by optical phonons, and deformation potential scattering of acoustic and optical phonons [42,43] have been considered, as listed below:

$$\tau_o = \frac{2\hbar^2 a^2 \rho(\hbar\omega_0)^2 (E + E^2/E_g)^{-1/2}}{\pi E_{oc}^2 k_B T (2m^*)^{3/2}(1 + 2E/E_g)\Theta} \tag{2a}$$

$$\tau_a = \frac{2\pi\hbar^4 C_l (E + E^2/E_g)^{-1/2}}{E_{ac}^2 k_B T (2m^*)^{3/2}(1 + 2E/E_g)\Theta} \tag{2b}$$

$$\Theta = 1 - \frac{8E/E_g(1 + E/E_g)}{3(1 + 2E/E_g)^2} \tag{2c}$$

$$\tau_{po} = \frac{(E + E^2/E_g)^{1/2}}{e^2(2m^*)^{1/2}k_B T(\varepsilon_\infty{}^{-1} - \varepsilon_0{}^{-1})(1 + 2E/E_g)} (1 - \delta\ln(1 + \delta^{-1}) - \frac{2E(E + E_g)}{(2E + E_g)^2}[1 - 2\delta + 2\delta^2\ln(1 + \delta^{-1})])^{-1}. \tag{2d}$$

In these equations, m^*, ε_∞, ε_0, Eg, a, ρ, ω_0, Cl, Eac and Eoc are the density-of-states effective mass, the high-frequency permittivity value, and static permittivity value, band gap, lattice constant, material density, optical phonon frequency, average elastic constant, the acoustic and optical deformation potential constants, respectively. Additionally, $\delta = (2kr_\infty)^{-2}$, with $r_\infty{}^{-2} = \frac{e^2}{\varepsilon_\infty}\int_0^\infty \left(-\frac{\partial f}{\partial E}\right) g(E)dE$. Values as listed in Table 1 (in Supplementary Material) are material constants used in above equations. More calculation details can be referred to our early study [26–28].

3 Results and discussions

The variations in unit-cell parameters after doping Ca/Sr/Ba atoms are shown in Figure 1. As shown in Figure 1a, after doping Ca atoms, the lattice parameters a, b and c all increase. However, the lattice parameters a and b increase but c decrease after doping Sr/Ba atoms. Moreover, it is worthwhile to note that the lattice parameters a and b are not equal after doping Ca/Sr/Ba, which indicates that dopants Ca/Sr/Ba greatly change the symmetry of the host. Nevertheless, the observed evolution of lattice parameter ratio a/c for all Ca/Sr/Ba-doped samples all increase, as shown in Figure 1b, which indicates that

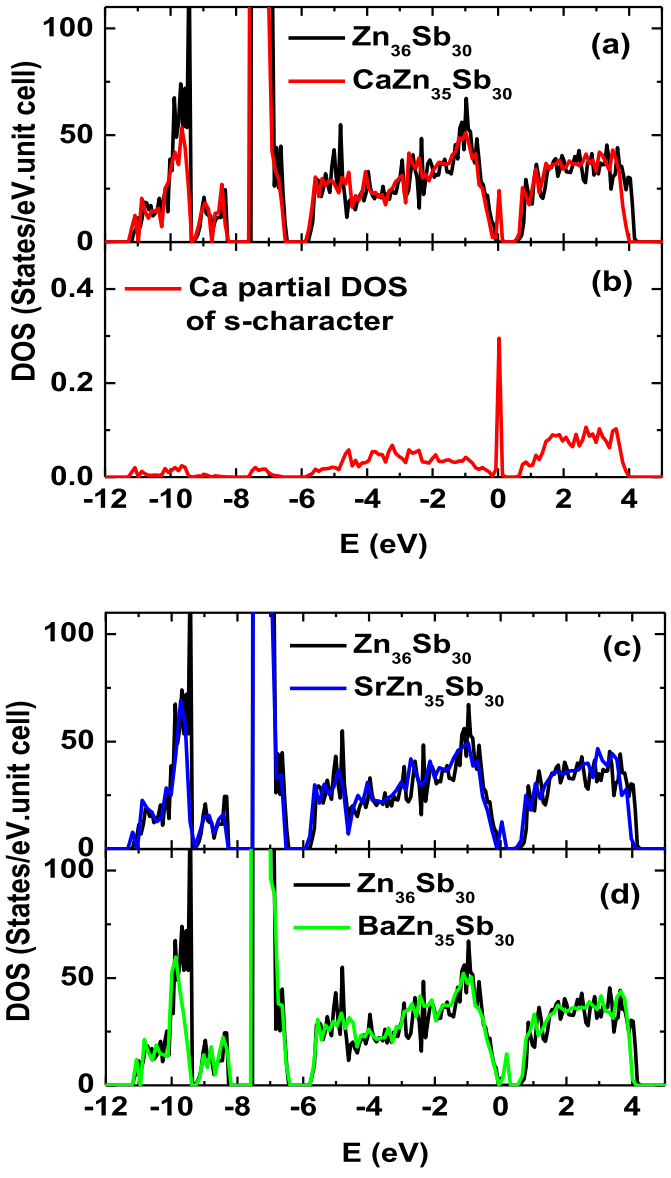

Fig. 2. (a) The TDOS of $Zn_{36}Sb_{30}$ without doping and doping Ca, (b) Ca PDOS of *s*-character, (c) the TDOS of $Zn_{36}Sb_{30}$ without doping and doping Sr, and (d) the TDOS of $Zn_{36}Sb_{30}$ without doping and doping Ba. The energy zero is set at the top of the valence band of the host.

dopants Ca/Sr/Ba are successfully introduced into the host, for Ca atom (atomic radius~ 2.23 Å), Sr atom (atomic radius~ 2.45 Å), or Ba atom (atomic radius~ 2.78 Å) are larger than Zn atom (atomic radius~ 1.53 Å), leading to expansion of the host lattice. It can be seen clearly how Ca/Sr/Ba atoms are incorporated into the host from Figures 2 and 3 of Supplementary Material.

The calculated DOS of $Zn_{36}Sb_{30}$ and $MZn_{35}Sb_{30}$ (M=Ca/Sr/Ba) were shown in Figure 2. $Zn_{36}Sb_{30}$ has a band gap of about 0.52 eV separating the valence band (VB) from conduction band (CB) with the Fermi energy E_F below the VB top ~0.35 eV. The DOS near E_F primarily composed of Zn-*s*, *p* and Sb-*p* states. The results are consistent with the earlier model calculations [44]. For the sake of comparison, we shifted the DOS of $MZn_{35}Sb_{30}$ (M=Ca/Sr/Ba) until the core bands at the lower edge of the valence band DOS match perfectly with that of $Zn_{36}Sb_{30}$. The moving magnitude is ~0.41/0.42/0.36 eV. Figure 2a shows the DOS for Ca-doped system. It can be seen clearly that a high resonant peak appears at 0.031 eV above the valence band maximum in the DOS of the host band. According to the formation energies E_{form} defined as the following equation [26,28],

$$E_{form} = E_{doped} + \mu_{Zn} - E_{undoped} - \mu_{Ca/Sr/Ba} \quad (3)$$

(E_{doped}, $E_{undoped}$, and μ is the total free energy for the supercell containing the dopant (Ca/Sr/Ba), the total free energy for the undoped supercell, and the chemical potentials of the constituent elements, respectively.) one can deduce E_{form} of the Ca point defects is ~ −2.47 eV/atom. From the partial DOS shown in Figure 2b, it reveals that *s* levels of the Ca atoms are the main contributor of this

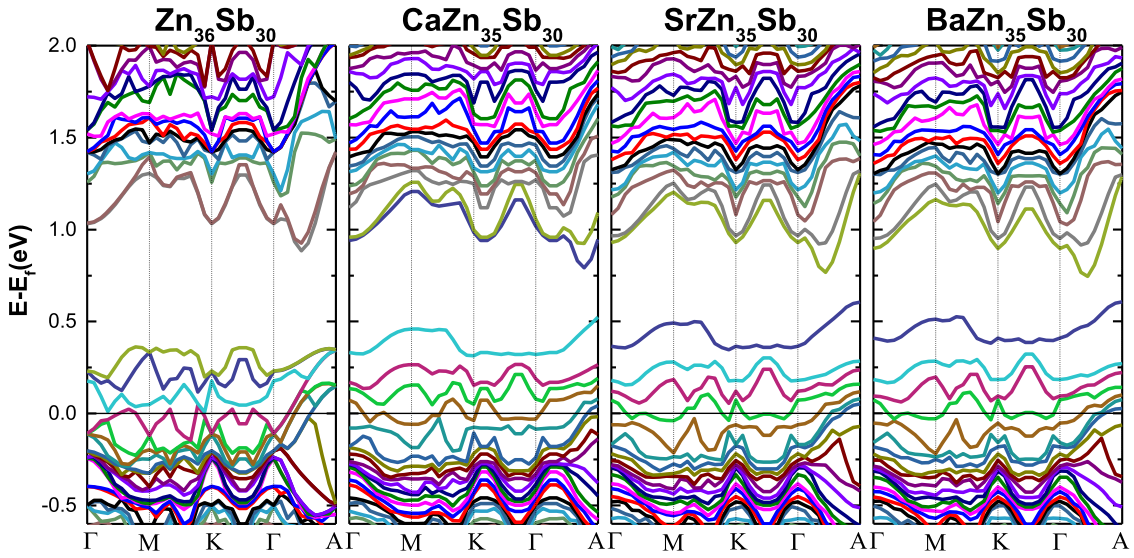

Fig. 3. The calculated band structures for $Zn_{36}Sb_{30}$ and defective configurations with Ca/Sr/Ba replacing Zn atoms along some high symmetry directions of the Brillouin zone. The energies are according to the Fermi-energy level shown by solid horizontal line.

peak. While for the Sr doping case as shown in Figure 2c, its corresponding formation energy is −2.25 eV/atom with a sharp peak and considerable enhancement in DOS above the top of the VB at 0.039 eV. As for Ba-doping case, which is shown in Figure 2d and corresponds to formation energy −2.47 eV/atom, it is similar to the cases of Ca and Sr doping when referring to a sharp peak at 0.185 eV and the slightly increased DOS near the top of VB.

These resonant peaks can be illustrated more clearly in the calculated band structure as shown in Figure 3. After doping one Ca/Sr/Ba atom in $Zn_{36}Sb_{30}$, the maximum valence band rises up at all the high symmetry points in the first Brillouin zone and splits off the original weakly degenerate band-edge states near the valence band maximum (VBM). The results indicate that the Ca/Sr/Ba atoms in $Zn_{36}Sb_{30}$ deviate from the ideal lattice positions (Fig. 1 of Supplementary Material) and reduce the symmetry of the Zn-Sb system. Meanwhile, Ca/Sr/Ba atoms in $Zn_{36}Sb_{30}$ bind weakly with the neighboring Sb atoms, and consequently, form band tail states.

The calculated room-temperature S and $\boldsymbol{\sigma}$ of $Zn_{36}Sb_{30}$ as a function of carrier concentration n are shown in Figure 4 of Supplementary Material. We can see that the calculated S and $\boldsymbol{\sigma}$ for the host have good agreement with the measured values in experiments [9,26–28,44].

The calculated $S, \boldsymbol{\sigma}$, and $S^2\boldsymbol{\sigma}$ of $MZn_{35}Sb_{30}$ (M=Ca/Sr/Ba) as a function of carrier concentration n are shown in Figure 4. As shown in Figure 4a, the calculated S of the four cases all increase in the entire studied carrier concentration as the carrier concentration decreases. The results show that Ca/Sr/Ba-doping brings significantly increase in Seebeck coefficient S. And nearly 8/9/19 times increase is achieved at $n \approx 7.0 \times 10^{27}$ m^{-3}, $n \approx 6.8 \times 10^{27}$ m^{-3}, and $n \approx 6.3 \times 10^{27}$ m^{-3} when doping Ca/Sr/Ba respectively.

Carrier concentration dependence of electrical conductivity $\boldsymbol{\sigma}$ of $MZn_{35}Sb_{30}$ (M=Ca/Sr/Ba) is displayed in Figure 4b. It can be seen that electrical conductivity for four cases all increase with increasing carrier concentration. However, the electrical conductivity of three doped structures is actually smaller than that of the host in the whole studied carrier concentration range. Consequently, because of increased S, as shown in Figure 4c, the largest power factor of three doping systems achieved here is about 10/4/2 times larger than that of the host at room temperature with $n \approx 7.1 \times 10^{27}$ m^{-3}, $n \approx 6.9 \times 10^{27}$ m^{-3}, and $n \approx 6.5 \times 10^{27}$ m^{-3}, respectively.

Figure 5a shows the carrier concentration dependence of the calculated carrier thermal conductivity λ_C of $MZn_{35}Sb_{30}$ (M=Ca/Sr/Ba). One can see that λ_C of $MZn_{35}Sb_{30}$ (M= Ca/Sr/Ba) all rise with carrier concentration increasing and greatly smaller than that of the host in the studied carrier concentration range, which is similar to the phenomenon observed in Figure 4b.

Figure 5b shows that room temperature ZT as a function of carrier concentration assuming $\lambda_L = 0.6 \mathrm{Wm^{-1}}K^{-1}$ (an average experimental value for pristine β-Zn_4Sb_3) for β-Zn_4Sb_3 doped with Ca/Sr/Ba. The maximum ZT 0.09/0.07 for the Ca/Sr-doped cases, both appear at $n \approx 7.0 \times 10^{27}$ m^{-3}, which is close to their values of n for optimal power factors. While the optimal ZT for Ba-doped case occurs at a smaller n, which is 0.1 at $n \approx 6.5 \times 10^{27}$ m^{-3}, locating just in the range of its optimizing power factor. Ultimately, the largest room temperature ZT values for three doping cases are about 14/12/8 times larger than that for the host at their corresponding carrier concentration, respectively. This increase in ZT is mainly owed to the increase of power factor and the simultaneous decrease of carrier thermal conductivity. If combining with other optimization methods to reduce lattice thermal conductivity simultaneously (such as nanostructure [45,47] or alloy scattering), we believe that further ZT enhancement can be obtained.

The carrier concentration $n(\mathrm{E_F})$ as a function of Fermi energy for $MZn_{35}Sb_{30}$ (M=Ca/Sr/Ba) at room temperature are shown in Figure 6. The carrier concentration can be calculated by using the following formula: $\mathrm{n(E)} = \int g(E) f(E)\, dE$, where $f(E)$ and $g(E)$ are the Fermi

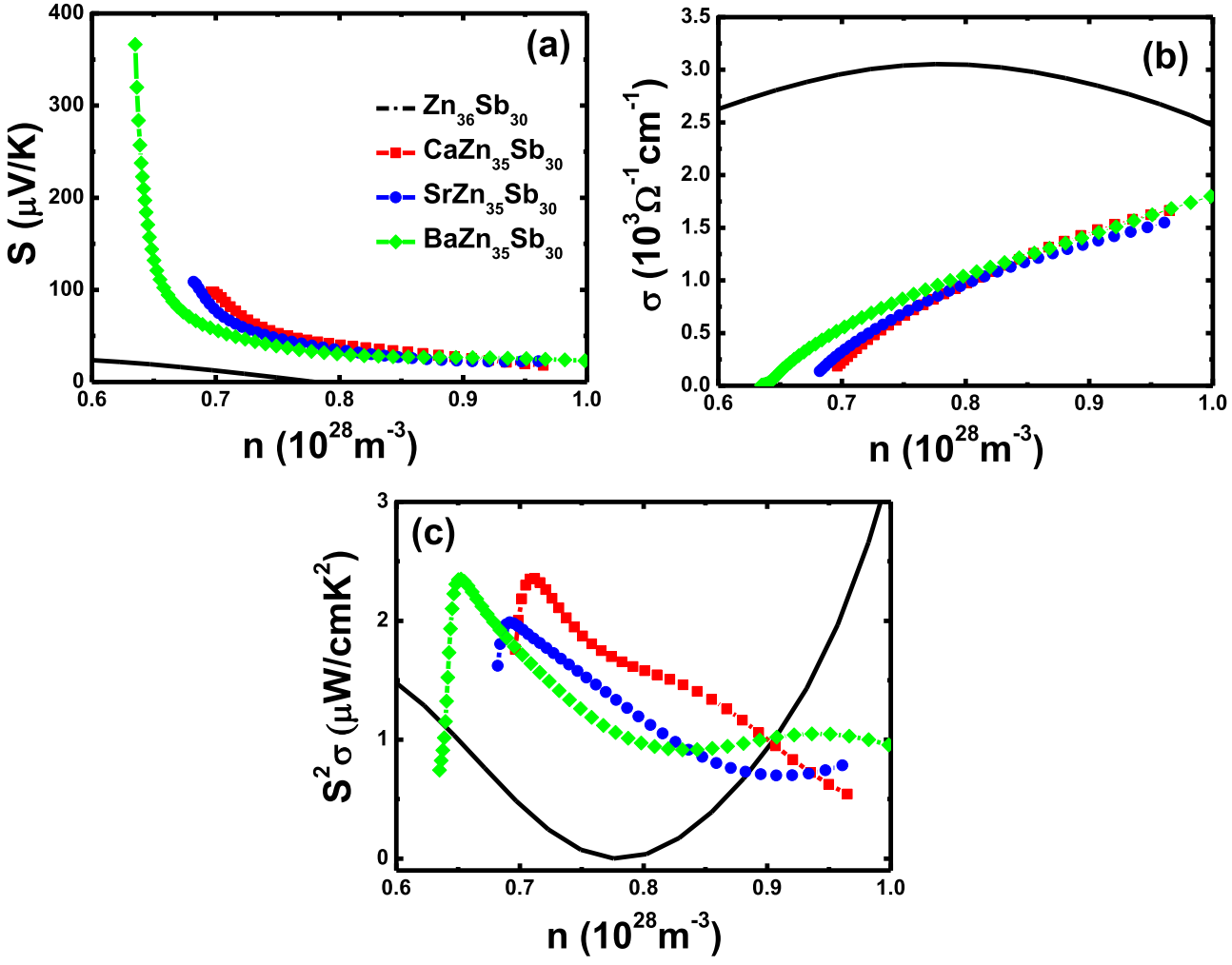

Fig. 4. The variation of thermoelectric properties for β-Zn_4Sb_3 doped with Ca/Sr/Ba with carrier concentration at $T = 300$ K. (a) Seebeck coefficient, (b) electrical conductivity, and (c) power factor.

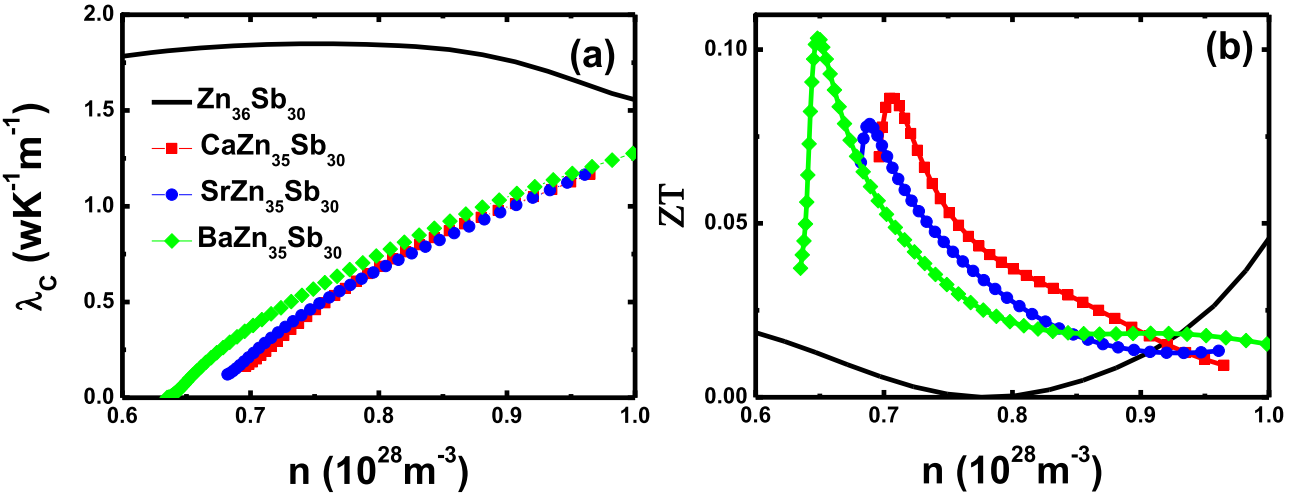

Fig. 5. The variation of thermoelectric properties for β-Zn_4Sb_3 doped with Ca/Sr/Ba with carrier concentration at $T = 300$ K. (a) Electronic thermal conductivity, (b) ZT values with $\lambda_L = 0.6\ Wm^{-1}\ K^{-1}$.

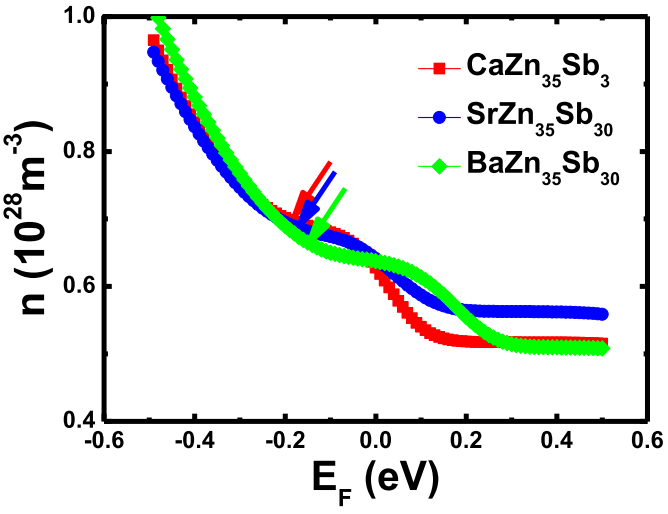

Fig. 6. The variation of carrier concentration for $MZn_{35}Sb_{30}$ (M = Ca/Sr/Ba) with Fermi energy at $T = 300$ K. The energy zero is set at the top of the valence band of the host. Arrows indicate where the best thermoelectric performance is achieved.

distribution function and the carrier density of states (DOS), respectively. As shown in Figure 6, n(Ca)≈n(Sr)≈n(Ba) as E_F is same. Thus, DOS(Ca)≈DOS(Sr)≈DOS(Ba) with an equal E_F can be derived, which is consistent with DOS calculation, electrical conductivity, and carrier thermal conductivity as shown in Figures 3, 4b, and 5a. As the largest ZT for $MZn_{35}Sb_{30}$ (M = Ca/Sr/Ba) at room temperature occur at $n \approx 7.0 \times 10^{27}$ m^{-3}, $n \approx 7.0 \times 10^{27}$ m^{-3} and 6.5×10^{26} m^{-3}, respectively, one can see that the corresponding optimal E_F values are E_F(Ca) = –0.21eV, E_F(Sr) = –0.21eV and E_F(Ba) = –0.09 eV, respectively, which are all near top of valence band. And this result is in good agreement with the recent reports concerning resonant states [48,49].

4 Conclusions

In this study, we have performed a systematic study on the alkaline-earth metal elements Ca, Sr and Ba doped β-Zn_4Sb_3 system. The results showed that Ca, Sr and Ba doping could lead to strong resonant effects in the DOS near the top of valence band, which can bring about a boost in Seebeck coefficient, and a degraded conductivity with a simultaneous decrease in carrier thermal conductivity. Overall, present results demonstrate that doping Ba is an effective method to elevate the thermoelectric performance of β-Zn_4Sb_3 with an optimal room-temperature $ZT = 0.1$ at $n \approx 6.5 \times 10^{27}$ m^{-3}.

Data availability

The authors indicate that the generated and analyzed data that support the findings of this study are available within the paper and the supplementary material.

The authors declare that they have no known competing financial interests or personal relationships that could have appeared to influence the work reported in this paper.

The authors acknowledge the Center for Computational Science, Hefei Institutes of Physical Sciences, Program for Innovative Research Team (in Science and Technology) in University of Yunnan Province, and the National Natural Science Foundation of China for financial support (Grants No. 52062044, 11674322, 51972307, and 1217040291).

Supplementary material

Supplementary Material provided by the author.
The Supplementary Material is available at https://www.epjap.org/0.1051/epjap/2022210237/olm.

Author contribution statement

M. Liu performed the first-principles electronic structure calculations and the numerical calculations. X.Y. Qin supervised the study. All authors participated in the analysis of the results and writing of the manuscript.

References

1. B.C. Sales, D. Mandrus, R.K. Williams, Science **272**, 1325 (1996)
2. R. Venkatasubramanian, E. Siivola, T. Colpitts, B. O'Quinn, Nature **413**, 597 (2001)
3. G. Mahan, B. Sales, J. Sharp, Phys. Today **50**, 42 (1997)
4. T.M. Tritt, Science **272**, 1276 (1996)
5. T.M. Tritt, Science **283**, 804 (1999)
6. S.K. Bux, R.G. Blair, P.K. Gogna, H. Lee, G. Chen, M.S. Dresselhaus, R.B. Kaner, J.-P. Fleurial, Adv. Funct. Mater. **19**, 2445 (2009)
7. F. Gascoin, S. Ottensmann, D. Stark, S.M. Haïle, G. Jeffrey Snyder, Adv. Funct. Mater. **15**, 1860 (2005)
8. Y. Pei, J. Lensch-Falk, E.S. Toberer, D.L. Medlin, G. Jeffrey Snyder, Adv. Funct. Mater. **21**, 241 (2011)
9. Y. Wu, J. Nylén, C. Naseyowma, N. Newman, F.J. Garcia-Garcia, U. Häussermann, Chem. Mater. **21**, 151 (2009)
10. T. Caillat, J.-P. Fleurial, A. Borshchevsky, J. Phys. Chem. Solids **58**, 1119 (1997)
11. G.J. Snyder, M. Christensen, E. Nishibor, T. Caillat, B.B. Iversen, Nat. Mater. **3**, 458 (2004)
12. F. Cargnoni, E. Nishibori, P. Rabiller, L. Bertini, G.J. Snyder, M. Christensen, C. Gatti, B.B. Iversen, Chem. Eur. J. **10**, 3861 (2004)
13. W. Schweika, R.P. Hermann, M. Prager, J. Perßon, V. Keppens, Phys. Rev. Lett. **99**, 125501 (2007)
14. A.P. Litvinchuk, J. Nylén, B. Lorenz, A.M. Guloy, U. Häussermann, J. Appl. Phys. **103**, 123524 (2008)
15. T. Koyanagi, K. Hino, Y. Nagamoto, H. Yoshitake, K. Kishimoto, in *16th International Conference on Thermoelectrics* (1997), p. 463
16. T. Caillat, J.-P. Fleurial, IEEE **2**, 905 (1996)
17. K.-W. Jang, I.-H. Kim, J.-I. Lee, G.-S. Choi, Int. Conf. Thermoelect. **129** (2005)
18. J.L. Cui, L.D. Mao, D.Y. Chen, X. Qian, X.L. Liu, W. Yang, Curr. Appl. Phys. **9**, 713 (2008)
19. J.L. Cui, H. Fu, D.Y. Chen, L.D. Mao, X.L. Liu, W. Yang, Mater. Charact. **60**, 824 (2009)
20. D. Li, H.H. Hong, J. Ma, X.Y. Qin, J. Mater. Res. **24**, 430 (2009)

21. F. Liu, X.Y. Qin, D. Li, J. Phys. D: Appl. Phys. **40**, 4974 (2007)
22. F. Liu, X.Y. Qin, H X Xin, J. Phys. D: Appl. Phys. **40**, 7811 (2007)
23. G. Nakamotom, T. Souma, M. Yamaba, M. Kurisu. J. Alloys Compd. **377**, 59 (2004)
24. B.L. Pedersen, H. Birkedal, E. Nishibori, A. Bentien, M. Sakata, M. Nygren, P.T. Frederiksen, B.B. Iversen, Chem. Mater. **19**, 6304 (2007)
25. B.L. Pedersen, H. Birkedal, M. Nygren, P.T. Frederiksen, B. B. Iversen, J. Appl. Phys. **105**, 013517 (2009)
26. M. Liu, X.Y. Qin, C.S. Liu, L. Pan, H.X. Xin, Phys. Rev. B **81**, 245215 (2010)
27. X.Y. Qin, M. Liu, L. Pan, H.X. Xin, J.H. Sun, Q.Q. Wang, J. Appl. Phys. **109**, 033714 (2011)
28. M. Liu, X. Qin, C. Liu, X. Li, X. Yang, J. Alloys Compd. **584**, 244 (2014)
29. T. Zou, X. Qin, Y. Zhang, X. Li, Z. Zeng, D. Li, J. Zhang, H. Xin, W. Xie, A. Weidenkaff, Sci. Rep. **5**, 17803 (2015)
30. J. Nylén, S. Lidin, M. Andersson, B.B. Iversen, H. Liu, N. Newman, U. Häussermann, Chem. Mater. **19**, 834 (2007)
31. Y.A. Ugai, E.M. Averbakh, V.V. Lavrov, Sov. Phys. Solid State **4**, 2393 (1963)
32. V.I. Psarev, N.L. Kostur, Izv. Vyssh, Uchebn. Zaved, Fiz. **10**, 34 (1967)
33. Y.A. Ugai, T.A. Marshakova, V.Y. Shevchenko, N.P. Demina, Inorg. Mater. **5**, 1381 (1969)
34. J. Nylén, M. Andersson, S. Lidin, U. Häussermann, J. Am. Chem. Soc. **126**, 16306 (2004)
35. A.S. Mikhaylushkin, J. Nylén, U. Häussermann, Chem. Eur. J. **11**, 4912 (2005)
36. J. Nylén, S. Lidin, M. Andersson, H. Liu, N. Newman, U. Häussermann, J. Solid State Chem. **180**, 2603 (2007)
37. P.E. Blöchl, Phys. Rev. B **50**, 17953 (1994)
38. G. Kresse, D. Joubert, Phys. Rev. B **59**, 1758 (1999)
39. J.P. Perdew, K. Burke, M. Ernzerhof, Phys. Rev. Lett. **77**, 3865 (1996)
40. D.M. Rowe, C.M. Bhandari, Modern Thermoelectrics (Holt Saunders, London, 1983)
41. J. Yang, H. Li, T. Wu, W. Zhang, L. Chen, J. Yang, Adv. Funct. Mater. **18**, 2880 (2008)
42. B.R. Nag, in *Electron Transport in Compound Semiconductors* (Springer-Verlag, Berlin, 1980), pp. 93–128
43. G.S. Nolas, J.W. Sharp, H.J. Goldsmid, *Thermoelectrics: Basics Principles and New Materials Developments* (Springer-Verlag, Heidelberg, 2001)
44. E.S. Toberer, P. Rauwel, S. Gariel, J. Taftøb, G. Jeffrey Snyder, J. Mater. Chem. **20**, 9877 (2010)
45. J. He, S.N. Girard, M.G. Kanatzidis, V.P. Dravid, Adv. Funct. Mater. **20**, 764 (2010)
46. B.A. Cook, M.J. Kramer, J.L. Harringa, M.-K. Han, D.-Y. Chung, M.G. Kanatzidis, Adv. Funct. Mater. **19**, 1254 (2009)
47. M. S. Toprak, C. Stiewe, D. Platzek, S. Williams, L. Bertini, E. Müller, C. Gatti, Y. Zhang, M. Rowe, M. Muhammed, Adv. Funct. Mat. **14**, 1189 (2004)
48. M. Liu, X.Y. Qin, C.S. Liu, Z. Zeng, Appl. Phys. Lett. **99**, 062112 (2011)
49. S. Thebaud, Ch. Adessi, S. Pailhes, G. Bouzerar, Phys. Rev. B **96**, 075201 (2017)

Cite this article as: Mian Liu, Changsong Liu, Xiaoying Qin, The effects of alkaline-earth-metal-element doping on the thermoelectric properties of β-Zn_4Sb_3, Eur. Phys. J. Appl. Phys. **97**, 21 (2022)